Novel Design of Two-tier Slotted-ALOHA OWC/RF IoT Networks with Adaptive Control

Milica Petkovic*, Anna Maria Vegni†, Enrique Hernandez Orallo‡, Pietro Manzoni‡, and Dejan Vukobratovic*
*Faculty of Technical Sciences, University of Novi Sad, Serbia, milica.petkovic@uns.ac.rs, dejanv@uns.ac.rs
†Dept. of Industrial, Electronic and Mechanical Engineering, Roma Tre University, Italy, annamaria.vegni@uniroma3.it
‡Universitat Politècnica de València, Spain, ehernandez@disca.upv.es, pmanzoni@disca.upv.es

***Abstract*—In this work, we present a novel design of a two-tier slotted-ALOHA system for massive Internet of Things (IoT) systems. Indoor IoT devices access the network via optical wireless communication (OWC), and relay data via a back-haul radio frequency low-power wide-area network (LPWAN). The main motivation of system under consideration is to reduce the connection density of LPWANs by offloading indoor devices to the OWC-based IoT. The first OWC tier employs slotted-ALOHA random access protocol with multi-packet reception and capture effect in the presence of interfering users, while the second LPWAN is based on slotted-ALOHA with different slot rates compared to the OWC tier. The aim of the presented analysis is to offer design insights for the two-tier OWC/RF system, while focusing on the adaptive selection of the data rates of OWC and LPWAN networks.**

***Index Terms*—Internet of Things, Low-Power Wide-Area Network, Optical Wireless Communications, Slotted ALOHA.**

I. Introduction

A range of wireless communication methods are included in traditional radio frequency (RF) Internet of Things (IoT) systems, intended to connect and exchange data between devices and systems over different distances. As an example of low-power wide area networks (LPWAN), LoRa (Long Range) plays a crucial role in this field with its long-range, low-power communication capabilities [1]. This technology is particularly favored for applications that require devices to transmit small amounts of data over long distances with minimal power consumption. LoRa technology uses sub-gigahertz frequencies for operation, and uses a spread spectrum modulation technology, which improves its capacity to sustain stable communication across extended distances under challenging settings [2], [3].

Optical wireless communication (OWC) [4] is a candidate technology for next generation wireless networks, and exploits optical carriers for data transmission, thus complementing high-frequency technology. It includes Li-Fi, infrared (IR), and visible light communication (VLC) technologies. Since light cannot penetrate opaque buildings and communication occurs in a room or other controlled location, OWC is characterized by high data throughput, energy efficiency, and improved security features. In the IoT context, OWC can enable fast, secure, and energy-efficient data transmission in situations that require high bandwidth, such as large sensor networks or densely populated urban areas, or in situations where RF communication may be less successful [5]–[7].

The goal of hybrid OWC/RF IoT systems is to combine the advantages of both technologies, that is (*i*) the fast and secure data transmission of OWC and (*ii*) the long-range and low power consumption of RF. The combination of both technologies has been the subject of recent studies, which have proposed designs that use OWC for secure, high-throughput local communication together with RF for long-range coverage [8]–[12]. In [8] Abuella *et al.* provide an overview of this field focusing on dynamic, reconfigurable networks that integrate RF and VLC, offering benefits like stable channels, enhanced mobility and security, reduced RF interference, and improved power efficiency, delay, and capacity. The authors in [9] explore the reduction in power in indoor wireless networks using VLC and WiFi for efficient dual-purpose communication and lighting, optimized to minimize power while meeting user and illumination needs. Simulations show that the hybrid system can save over 75% in power compared to standalone WiFi or VLC systems. In [10] the authors develop a hybrid cellular architecture for the IoT, enabling interoperability between technologies such as ZigBee, LoRaWAN, and VLC to enhance coverage in remote areas. Field tests demonstrate the architecture's ability to facilitate long-range, high-rate data transmission across diverse wireless technologies, proving its efficacy in rural and isolated environments. Finally, in [11], [12], a hybrid OWC/RF system consisting of indoor OWC and outdoor LPWAN IoT systems employed for the slotted ALOHA (SA)-based uplink communications is analyzed. More precisely, the work in [11] analyzes the packet loss rate of the hybrid OWC/RF system by utilizing stochastic geometry approach, while in [12] a novel design of OWC/RF system has been investigated, consisting of a set of indoor OWC IoT systems connected to a network infrastructure via LPWAN RF-based IoT systems.

Inspired by the novel hybrid OWC/RF architecture for future massive IoT proposed in [12], we extend the analysis to the novel framework where LoRa layer is adopted to control OWC sub-systems. A set of OWC systems are considered for the first indoor tier, which are connected to a LoRa base station (BS) via outdoor LPWAN RF-based IoT systems. Both the indoor and outdoor IoT systems employ SA-based random access policy. The second-tier RF transmission is based on the SA with the slot rate different than those of indoor OWC IoT systems. The contribution of the paper is summarized as follows:

- Differently from [12], we consider the OWC interference contribution into the derivation of the overall system throughput. As the frequency reuse approach is adopted in all OWC IoT devices, the received optical signals (except the reference one) are considered to be interference [13], which has to be taken into account during analysis;
- Based on presented numerical results, we provide detailed analysis of the achieved throughput performance, considering different parameters of both OWC and RF systems;
- We upgrade the proposed system by employing an adaptive control of the achieved performance. Specifically, by accordingly controlling the multi-rate factor, which affects the slot rate (*i.e.*, data rate) of both RF and OWC tiers, it results a maximal achievable throughput performance for different system setups.

The rest of this paper is organized as follows. Section II describes in details the system model for the proposed two-tier OWC/RF IoT scenario. The assessment of the achieved performance, expressed as throughput, are then presented in Section III. Finally, conclusions are drawn at the end of the paper.

II. System and Channel

Fig. 1 depicts the overall hybrid OWC/RF IoT scenario. It is comprised of two tiers *i.e.*, (*i*) an indoor OWC-based IoT, and (*ii*) an outdoor LPWAN RF-based IoT network layer. The first OWC IoT layer considers a collection of K OWC IoT systems distributed across a wide area, each comprised of U OWC IoT devices uniformly distributed over the same horizontal plane within a circular coverage area of radius R [m], and one OWC access point (AP) positioned at a height L [m] above the center of the circular area. The AP emits the optical intensity with a given field-of-view (FOV).

At each OWC system, the SA random access policy is adopted to provide the access of total U IoT devices to the OWC AP. In each slot, the OWC IoT devices transmit a fixed-length data packet with activation probability p_a during a slot of duration defined as T_{owc} [s]. The OWC AP is trying to recover and decode data packets from the received signal, acting as decode and forward (DF) relay to further forward decoded packets to the RF BS. The SA approach adopts the capture effect and multi-packet reception (MPR) strategy, thus the considered receiver model for OWC AP will be able to decode multiple packets originating at multiple active devices by exploiting the capture effect based on interference contribution.

The second RF tier considers the connection of K OWC APs to the BS via a outdoor LPWAN RF-based network. In this layer, the SA scheme has a slot duration T_{rf} [s]. In order to improve robustness against interference and multipath fading, the outdoor LPWAN is based on LoRa physical layer, which employs a chirp spread spectrum (CSS) modulation scheme [3]. The CSS modulation is convenient as it employs quasi-orthogonal spreading factors (SFs), ensuring that users with different SFs will generate minimal inter-SF interference to each other [3], [14]. Based on the distance between

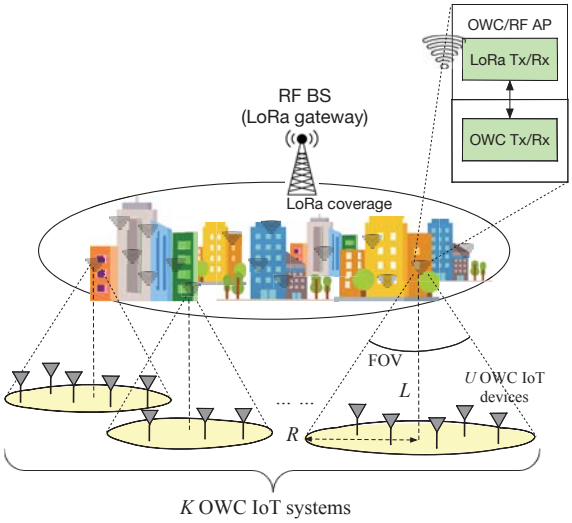

Fig. 1. Schematic of the two-tier OWC/RF IoT system.

the LoRa BS and the i-th OWC IoT AP *i.e.*, d_{SF} [m], the BS is responsible for assigning the spreading factor SF $\in \{7, 8, \ldots, 12\}$, while keeping the constant bandwidth (BW). When LoRa users are at closer distances from the BS, the lower SF will be assigned, resulting in higher data rates, shorter chirp symbol, reduced reception sensitivity, and lower processing gain. The relationship between the chirp symbol duration, the SF, and the bandwidth is as follows [3]:

$$T_s = 2^{\text{SF}}/\text{BW}. \tag{1}$$

Furthermore, in order to provide more realistic insights into performance of the proposed two-tier OWC/RF-based IoT network, we adopt the model where successfully decoded packets in the first OWC tier, acting as LoRa users, will be forwarded at the same SF to the LoRa BS. In other words, all K OWC APs are positioned at the approximate same distance d_{SF} [m] from the LoRa BS.

According to the system model in [12], we consider the following relationship between the slot duration in the OWC layer (*i.e.*, T_{owc}) and the LoRA RF slot duration (*i.e.*, T_{rf})

$$T_{\text{owc}} = M \cdot T_{\text{rf}}, \quad M \in \mathbb{N}/0, \tag{2}$$

where M is defined as multi-rate factor. Since LoRa BS is able to perform adjustment and adaptive control of multi-rate factor M, by assigning the SF, the LoRa BS adequately controls the slot rate as $T_{\text{owc}} = M \cdot T_{\text{rf}}$ and data rate of the OWC systems. This approach allows the LoRa network to maintain a consistent BW, while offering adaptive data rates based on M adjustment within the end-to-end system model.

In the following subsections, we provide more details of each IoT tier.

A. Indoor OWC-based IoT Network

In each of the K OWC systems, U IoT devices are uniformly placed on a horizontal plane. The SA random access scheme with Bernoulli arrivals is used to model the number

of active users distribution in a each slot, meaning that each of U IoT devices becomes activated in a given slot with probability p_a independently of any other user. For the i-th OWC IoT system (*i.e.*, $i = 1, \ldots, K$), $U_a^{(i)}$ defines the number of activated users, being a binomial random variable with mean Up_a, which leads to the probability

$$\mathbb{P}[U_a^{(i)} = u] = \binom{U}{u} p_a^u (1 - p_a)^{U-u}. \tag{3}$$

All OWC-based transmitters employ LED operating in the IR spectrum and employing intensity modulation with on-off keying to satisfy non-negative constraint. All OWC APs include OWC receivers, *i.e.*, photodetectors, employing direct detection for optical signal reception. Only line-of-sight (LoS) links between IoT devices and OWC AP are considered, since the energy from the reflected signals can be neglected as it is significantly lower than the energy of the LoS component [15].

The location of the j-th OWC IoT device with respect to the i-th OWC AP (with $i = 1, \ldots, K$, and $j = 1, \ldots, U_a^{(i)}$) can be determined by the angle of irradiance θ_j from the i-th OWC AP, the angle of incidence ψ_j to the j-th IoT device, and the Euclidean distance among them, *i.e.*, $d_{i,j}$ [m]. We adopt a Lambertian law for modeling the optical LoS link, thus the intensity of the received optical signal between the i-th OWC AP and the j-th OWC IoT device, can be defined as [4]

$$h_{i,j} = \begin{cases} \frac{A(m+1)T_g g(\psi_{i,j})}{2\pi d_{i,j}^2} \cos^m(\theta_j) \cos(\psi_j), & 0 \leq \psi_{i,j} \leq \Psi \\ 0, & \text{otherwise} \end{cases} \tag{4}$$

where A [cm]^2 represents the physical area of the detector, T_g is the gain of the optical filter, $g(\psi_{i,j}) = l^2 / \sin^2(\Psi)$, for $0 \leq \psi_{i,j} \leq \Psi$, is the the optical concentrator with the refractive index of lens at a photodetector denoted by l, and Ψ denotes the field-of-view (FoV) of the receiver. The Lambertian order of the light source is determined as $m = -\ln 2 / \ln\left(\cos \Phi_{1/2}\right)$, where $\Phi_{1/2}$ represents the semi-angle at half power of LED.

Following the aforementioned model, the signal-to-noise ratio (SNR) of the OWC link between the i-the OWC AP and the j-th OWC IoT device can be defined as

$$\gamma_{\text{owc}}^{i,j} = \frac{P_t^2 \eta^2 h_{i,j}^2}{\sigma_n^2}, \tag{5}$$

where η is the optical-to-electrical conversion coefficient, P_t represents the transmitted optical power, and $\sigma_n^2 = N_0 B$ is the Gaussian noise variance with N_0 and B being the noise spectral density and the system bandwidth, respectively. Also, since the same frequency is reused in all IoT devices within OWC indoor system, the signals received from all users except the reference one are considered to be an interference. It follows that for the i-th OWC system, the signal-to-interference-noise ratio (SINR) for the j-th user can be defined as [16]

$$\text{SINR}_{\text{owc}}^{i,j} = \frac{\gamma_{\text{owc}}^{i,j}}{\sum_{\substack{n=1 \\ n \neq j}}^{U_a^{(i)}} \gamma_{\text{owc}}^{i,n} + 1}, \tag{6}$$

TABLE I
LoRa characteristics [3]

SF	Bit-rate [kbps]	T_{rf} [ms]	q_{SF}	d_{SF} [km]
7	5.47	36.6	-6	1 ± 1
8	3.13	64	-9	3 ± 1
9	1.76	113	-12	5 ± 1
10	0.98	204	-15	7 ± 1
11	0.54	372	-17.5	9 ± 1
12	0.29	682	-20	11 ± 1

where $\sum_{\substack{n=1 \\ n \neq j}}^{U_a^{(i)}} \gamma_{\text{owc}}^{i,n}$ represents the interference contribution. More details about derivation of the SINR statistics in indoor uplink OWC system can be found in [16].

Finally, in the indoor OWC tier we adopt the SA policy with (*i*) capture effect and (*ii*) MPR possibility. Regarding the capture effect, a packet can be decoded only if the received SINR at the j-th user *i.e.*, $\text{SINR}_{\text{owc}}^{i,j}$, is above a previously determined threshold, denoted by γ_{th}. The error probability that a packet will not be decoded can be defined as

$$\text{P}_{\text{er}} = \mathbb{P}\left[\text{SINR}_{\text{owc}}^{i,j} < \gamma_{\text{th}}\right]. \tag{7}$$

Regarding the MPR possibility, multiple packets from multiple active devices can be decoded by the i-th OWC AP within the same OWC IoT system. As the ratio M between slot duration in OWC and RF tiers impacts the maximal load of the LPWAN RF network, we define M to be the maximal number of packets possibly decoded at each OWC AP. Further, the packets with higher received power have priority over the possibility to be decoded. It means that maximal number of decoded packets in each OWC system, which will be further forwarded via the second tier, is equal to M, determining the load of the LPWAN RF network. As the i-th OWC AP acts as DF relay, it will forward data packets to the outdoor BS during the assigned slot of duration T_{rf}, by following the SA approach.

B. Outdoor LPWAN RF-based IoT Network

As the slot rate at the RF system is M times smaller than T_{owc}, the decoded packet at the i-th OWC AP will be transmitted within M newly formed slots at the second tier (in parallel with one OWC slot). Notice that only a single packet can be allocated to each of the newly formed slots.

The overall load, *i.e.*, the number of active devices, of the LPWAN RF network is determined by the value of M and the number of decoded packets at the OWC IoT systems. Based on the distance d_{SF} [m], the LoRa BS adjusts the SF, which determines a bit-rate, the time-on-air of a transmission and receiver sensitivity determined by the threshold q_{SF}. For different SF, values of these parameters are presented in Table I [3]. As previously mentioned, the choice of SF will determine the RF slot duration T_{rf} [s], allowing the LoRa BS station to determine the slot rate T_{owc} in the OWC systems by performing adaptive control of parameter M (since $T_{\text{owc}} = M \cdot T_{\text{rf}}$).

After being successfully decoded and assigned to new RF mini slots, a packet is forwarded to LoRa gateway with

transmit power $P_{\rm rf}$ [W] over Rayleigh distributed block flat-fading channel. The instantaneous SNR can be defined as

$$\gamma_{\rm rf} = \frac{P_{\rm rf} g_{\rm SF} h_{\rm rf}^2}{\sigma_{\rm rf}^2}, \tag{8}$$

where $h_{\rm rf}$ is the fading amplitude of the RF link modeled by Rayleigh distribution, $g_{\rm SF}$ the path loss attenuation, while $\sigma_{\rm rf}^2$ represents the additive white gaussian noise variance determined as $\sigma_{\rm rf}^2 = -174 + {\rm NF} + 10{\rm log BW}$ [dBm], where NF is the receiver noise figure [3]. The path loss attenuation function is determined by the Friis transmission equation as $g_{\rm SF} = (\lambda/4\pi d_{\rm SF})^n$, where $d_{\rm SF}$[m] is the distance given in Table I, λ [nm] represents the carrier wavelength, and n is the path loss exponent to be equal to 2.7 and 4 in urban and sub-urban environments, respectively.

As the second RF tier is based on SA random access approach, a desired packet will be successfully decoded at the BS if outage does not happen. Following the outage conditions proposed in [3], we assume the outage will occur at the BS if at least of one of the following two conditions is satisfied:

1) The first outage condition: For assigned SF, the specific threshold $q_{\rm SF}$ is determined (see Table I). The instantaneous SNR of the received packet is below $q_{\rm SF}$, *i.e.*,

$$\mathrm{P}_{\rm o,1} = \mathbb{P}\left[\gamma_{\rm rf} < q_{\rm SF}\right] = \mathbb{P}\left[\frac{P_{\rm rf} g_{\rm SF} h_{\rm rf}^2}{\sigma_{\rm rf}^2} < q_{\rm SF}\right]. \tag{9}$$

Assuming Rayleigh distributed fading channel at the second tier, the first outage condition is determined as

$$\mathrm{P}_{\rm o,1} = \mathbb{P}\left[h_{\rm rf}^2 < \frac{\sigma_{\rm rf}^2 q_{\rm SF}}{P_{\rm rf} g_{\rm SF}}\right] = 1 - \exp\left(\frac{\sigma_{\rm rf}^2 q_{\rm SF}}{P_{\rm rf} g_{\rm SF}}\right). \tag{10}$$

2) The second outage condition: it requires that the desired signal will be the strongest one among all received signals with the same SF, as well as that it will be at least 4 times stronger than any other received signal, *i.e.*,

$$\mathrm{P}_{\rm o,2} = \mathbb{P}\left[\frac{\gamma_{\rm rf}}{\gamma_{\rm rf}^*} \leq 4\right], \tag{11}$$

where $\gamma_{\rm rf}^*$ defines the instantaneous SNR of interfering signal with the same SF.

The achieved throughput will be affected by the value of M *i.e.*, $\Theta(M)$. It can be observed that for increasing M, it is expected that the throughput will be higher. By comparing the achievable throughput to a quality threshold (*i.e.*, ρ), it is possible to perform an adaptive control of M in order to improve the throughput. Specifically, starting from a given M, we can define the adaptive-M parameter (*i.e.* $M^\star$) as

$$M^\star = M + 1, \tag{12}$$

if the following conditions hold:

$$\Theta(M) < \rho \ \ \text{AND} \ \ M \leq M_{\max}, \tag{13}$$

where $M_{\max}$ is the maximum value allowed for M (usually, $M_{\max} = 7$). As a result, the throughput achieved for $M^\star$ is expected to provide a gain over that one with fixed M.

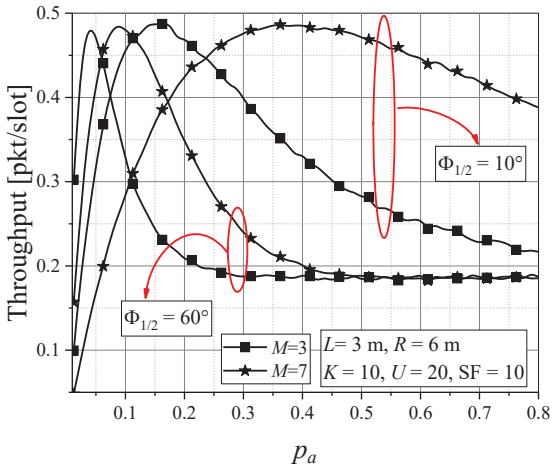

Fig. 2. Achieved throughput [pkt/slot] versus the activation probability, for different values of semi-angle $\Phi_{1/2}$ and M.

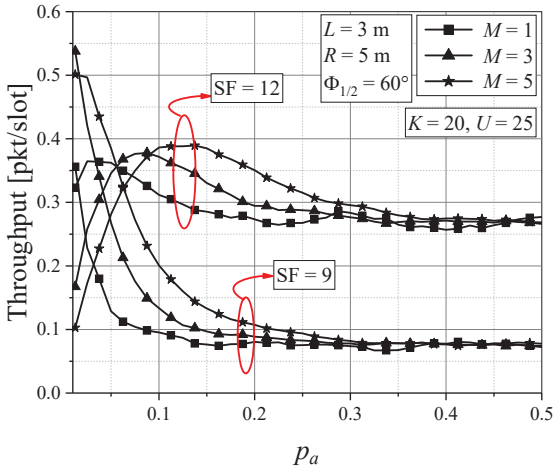

Fig. 3. Achieved throughput [pkt/slot] versus the activation probability, for different M.

III. Numerical Results

In this section, we show the numerical results of the achievable throughput in the considered hybrid system, obtained by Monte Carlo simulations via MatLab software. Specifically, we show the achievable throughput versus the user activation probability p_a, for different parameters such as the number of users U, the number of OWC APs K, the multi-rate factor M, the LoRa SF, and other OWC parameters like the half-power semi-angle, the AP's height and the radius.

Fig. 2 shows the trends of the achievable throughput versus the activation probability, for different values of the semi-angle $\Phi_{1/2}$ and M factor. It can be noted that for a given semi-angle, throughput performance can be improved for greater activation probability. In other words, the LoRa BS can select the optimal value of M in order to reach the maximal throughput for a certain number of active users determined by p_a. When the estimation of active probability is applied into OWC system, the LoRa BS can decide the optimal value of M in order to

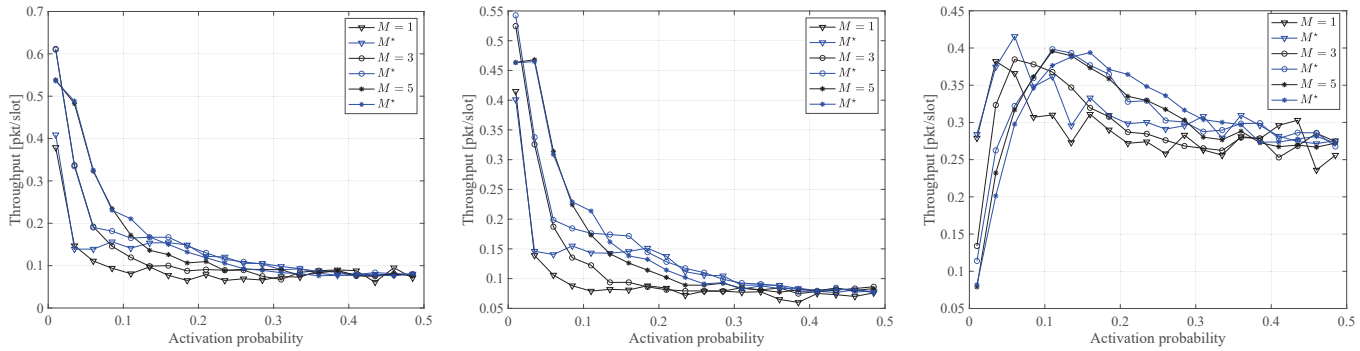

(*a*) (*b*) (*c*)

Fig. 4. Comparison of the achieved throughput versus the activation probability in case of $\rho = 0.3$, for different M and SF values *i.e.*, (*a*) SF $= 7$, (*b*) SF $= 9$, and (*c*) SF $= 12$. $M^\star$ represents the adaptive-M parameter defined in (12).

achieve the best system performance. Furthermore, it is evident that the semi-angle $\Phi_{1/2}$, as well as the geometry setup of the OWC system (including height L [m] and radius R [m]) has noteworthy impact on the system performance, and should be assessed in order to optimize the performance of the random access protocol.

Fig. 3 depicts throughput dependence on p_a for different multi-rate parameter M, considering different SFs (*i.e.*, SF $= 9$ and SF $= 12$). The SFs are determined by distances between OWC systems and LoRa BS, and they affect the slot duration T_{rf}, while T_{owc} will be determined based on the value of assigned M. The maximal throughput can be achieved for optimal value of p_a, which differs for various combinations of SF and parameter M. It can be observed that for a given SF and activation probability, the throughput increases for higher values of M. It is obvious that, for a certain SF corresponding to a given distance between OWC systems and LoRa BS, the adaptive control of parameter M can be performed in order to achieve maximal throughput performance.

Leveraging on the previous results, we observe that the throughput reaches variable maximum values for different M. Increasing M allows having an improved throughput, especially for higher activation probability. This observation motivated us to consider an adaptive control on the parameter M, so that it will be changing if the throughput does not reach a fixed threshold *i.e.*, ρ. The achieved throughput with the adaptive-M approach is shown in Fig. 4 and Fig. 5 in case of $\rho = 0.3$ and 0.5, respectively. The adaptive control is activated when the throughput with a fixed M is lower than a given threshold ρ. Starting from a fixed M, the adaptive control increases M in order to reach the threshold ρ.

However, the achievement of threshold ρ is a slow process, specially when the gap between the initial throughput and ρ is larger. This can be easily observed in Fig. 4(c), where $\rho = 0.3$ and the initial throughput for a fixed M is smaller. For instance, for $M = 3$ the throughput is ≈ 0.13 for $p_a = 0.01$. The adaptive control increases the value of M in order to overcome the value of ρ. We observe a gain of throughput with the adaptive-M control, specially for high activation probability for $p_a > 0.1$; in contrast, for $p_a \leq 0.1$, the throughput for fixed M is higher than that of the adaptive-M approach. Similar considerations apply in case of $M = 5$, and the associated adaptive-M control will show higher throughput for $p_a > 0.18$. The gain will be maintained for increasing activation probability.

Notice that the adaptive-M technique is an attempt to improve the achievable throughput obtained in case of fixed M, which is expected to overcome a threshold ρ. However, the adaptive-M technique does not guarantee the gain of throughput over the threshold ρ, but it is possible to achieve an improvement of throughput over the case of fixed M. For instance, in Fig. 5 the curves obtained with the adaptive-M approach overcome those with fixed M, but are not able to reach the threshold of $\rho = 0.5$. This is due to a linear increase of M (*i.e.*, $M^\star = M + 1$), which is also limited to $M = 7$.

Finally, Fig. 6 shows the comparison of our results and results presented in [12]. Throughput vs. p_a is observed for the fixed $M = 5$. Two distances between OWC systems and LoRa BS are considered, resulting in SF $= 7$ and SF $= 11$. The proposed systems differs to [12] in the OWC system model, *i.e.*, we take into account interference of other OWC users (SINR should be greater than the threshold in order to decode the packet at OWC AP), while the approach in [12] considers this condition based on the SNR. From Fig. 6 it can be observed that novel approach gives the better throughput performance for lower values of activation probability (which is more common situation in massive IoT systems). As K OWC APs contend for the access to the LoRA BS, the overall decoded packets at the OWC systems will determine the overall load at the RF tier. For greater p_a, number of active users at OWC systems is higher, leading to the strong interference contribution, which results in small number of decoded packets at the OWC APs (very low throughput of the proposed system). On the other hand, smaller p_a, *i.e.*, lower number of active users at OWC systems reflects in the weak interference contribution, which means that not all of K OWC AP will decode the packets, but still some of them will be successfully decoded and forwarder to the LoRa BS.

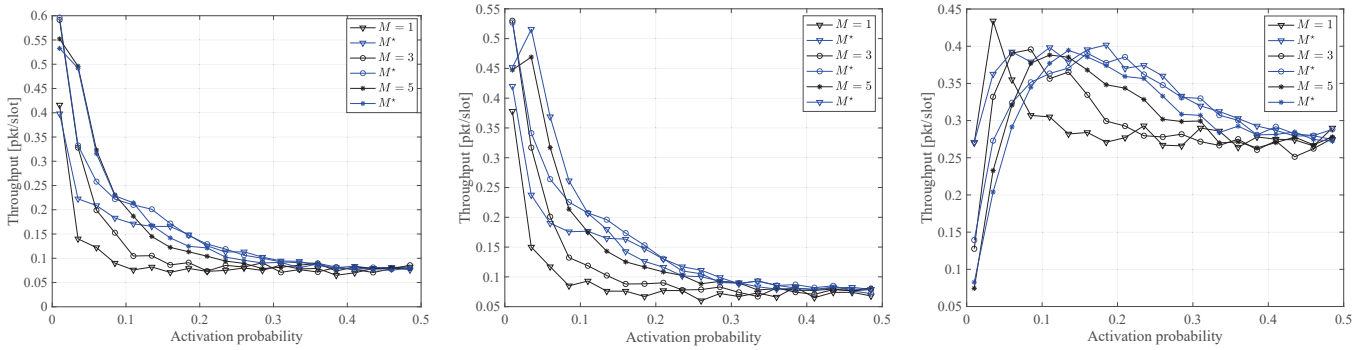

(*a*) (*b*) (*c*)

Fig. 5. Comparison of the achieved throughput versus the activation probability in case of $\rho = 0.5$, for different M and SF values *i.e.*, (*a*) SF $= 7$, (*b*) SF $= 9$, and (*c*) SF $= 12$. $M^\star$ represents the adaptive-*M* parameter defined in (12).

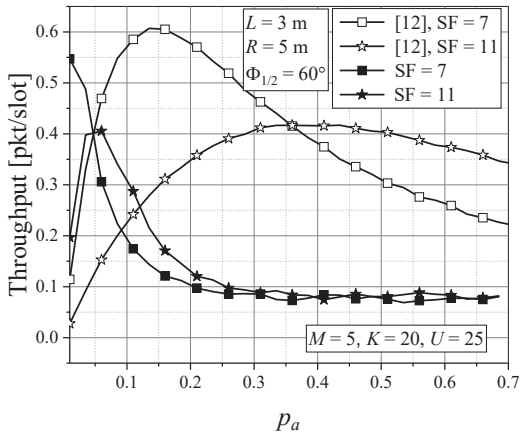

Fig. 6. Comparison of the achieved throughput [pkt/slot] in case of (*i*) our proposed approach, and (*ii*) that presented in [12].

Contrary, when there is no interference as proposed in [12], most of the K OWC APs will decode the packets, resulting in very high load at the second tier and the traffic congestion. To conclude, for lower values of p_a, the load at the second RF tier in proposed system is lower than the one presented in [12], leading to the improved overall throughput performance.

IV. Conclusions

This paper presented a novel two-tier hybrid OWC/RF IoT framework. The proposed architecture aims to reduce the connectivity density of RF IoT systems by offloading indoor devices to OWC IoT layer. The investigation of network performance has been carried out taking into account the interference contribution coming from multiple user transmission in a SA random access technique. Also, an adaptive control on the multirate factor has been introduced in order to enhance the achievable throughput for the end-to-end system.

Acknowledgment

This work has received funding from the Horizon 2020 research and innovation staff exchange grant agreement No 101086387. This article was based upon work from COST Action NEWFOCUS CA19111, supported by COST (European Cooperation in Science and Technology).

References

[1] M. L. Liya and M. Aswathy, "LoRa technology for Internet of Things(IoT): A brief Survey," in *Proc. 2020 Fourth International Conference on I-SMAC*, Palladam, India, 2020, pp. 8-13.

[2] A. Zourmand, A. L. Kun Hing, C. Wai Hung, and M. AbdulRehman, "Internet of Things (IoT) using LoRa technology," in *Proc. I2CACIS 2019*, Selangor, Malaysia, 2019, pp. 324-330.,

[3] O. Georgiou and U. Raza, "Low Power Wide Area Network analysis: Can LoRa scale?," *IEEE Wireless Commun. Lett.*, vol. 6, no. 2, 2017.

[4] Z. Ghassemlooy, W. Popoola, and S. Rajbhandari, *Optical Wireless Communications: System and Channel Modelling With MATLAB*. Boca Raton, FL, USA: CRC Press, 2013.

[5] A. Celik, I. Romdhane, G. Kaddoum and A. M. Eltawil, "A Top-Down Survey on Optical Wireless Communications for the Internet of Things," *IEEE Commun. Surv. Tutor.*, vol. 25, no. 1, pp. 1-45, 2023.

[6] S. R. Teli, S. Zvanovec, and Z. Ghassemlooy, "Optical Internet of Things within 5G: Applications and Challenges," in *Proc. IOTAIS 2018*, Bali, Indonesia, 2018, pp. 40–45.

[7] M. Z. Chowdhury, et al., "The role of Optical Wireless Communication technologies in 5G/6G and IoT solutions: Prospects, Directions, and Challenges," *Appl. Sci.*, vol. 9, no. 20, 2019.

[8] H. Abuella et al., "Hybrid RF/VLC Systems: A Comprehensive Survey on Network Topologies, Performance Analyses, Applications, and Future Directions," in *IEEE Access*, vol. 9, pp. 160402-160436, 2021.

[9] A. Khreishah, et al., "A Hybrid RF-VLC System for Energy Efficient Wireless Access," in *IEEE Trans. Green Commun. Netw.*, vol. 2, no. 4, pp. 932-944, Dec. 2018.

[10] F. Delgado-Rajo, et al., "Hybrid RF/VLC Network Architecture for the Internet of Things," *Sensors*, vol. 20, no. 478, 2020.

[11] T. Devaja, M. Petkovic, A. Munari, F. Clazzer, M. Beko, and D. Vukobratovic "Massive Machine-Type Communications via Hybrid OWC/RF Networks," in *Proc. CSNDSP 2022*, Porto, Portugal, 2022.

[12] M. Petkovic, D. Vukobratovic, A. Munari, and F. Clazzer, "Two-Tier Multi-Rate Slotted ALOHA for OWC/RF-Based IoT Networks," *IEEE Commun. Lett.*, vol. 27, no. 4, pp. 1190-1194, April 2023.

[13] R. Ahmad, et al., "Reinforcement Learning Based Load Balancing for Hybrid LiFi WiFi Networks," *IEEE Access*, vol. 8, pp. 132273-132284, 2020.

[14] C. Goursaud, J.-M. Gorce, "Dedicated networks for IoT: PHY/MAC state of the art and challenges," *EAI endorsed TIoT*, 2015.

[15] M. B. Rahaim, A. M. Vegni and T. D. C. Little, "A hybrid Radio Frequency and broadcast Visible Light Communication system," in *Proc. of 2011 IEEE GLOBECOM Workshops (GC Wkshps)*, Houston, TX, USA, 2011, pp. 792-796.

[16] T. Devaja, M. Petković, F. J. Escribano, Č. Stefanović and D. Vukobratović, "Slotted Aloha With Capture for OWC-Based IoT: Finite Block-Length Performance Analysis," in *IEEE Access*, vol. 11, pp. 76804-76815, 2023.